A Method for the Analysis of Physical Human-Robot Interaction*

Saad N. Yousaf[1], Paria Esmatloo[1], Keya Ghonasgi[1], and Ashish D. Deshpande[1]

***Abstract*—Physical human-robot interaction (pHRI) interfaces are responsible for ensuring safe, comfortable, and effective force transfer between wearable devices and their users. However, analysis is often oversimplified by treating the human-robot attachment as a rigid connection and using gross load measurements. As a result, information about the distribution of forces across the human-robot contact surface is lost. In this paper, we present an analysis method to predict distributed loading across a pHRI interface based on a model with discretized elastic elements that account for compliance from human soft tissue and the robot attachment. Stiffness properties of a proxy upper arm are measured with an indenter and used in the pHRI interface model. The analysis is performed assuming a rigid arm model, consistent with the underlying assumption in literature, and repeated using the proposed compliant arm model with measured elastic properties. The distributed loading predicted by the pHRI interface model is validated with measurements from a sensorized upper arm cuff on the Harmony exoskeleton. Our results reveal that a model incorporating compliance at the human-robot attachment is necessary to improve prediction of distributed interface loads. This motivates the need for human-centered analysis which can enable finer control of interaction forces and help design more ergonomic attachment interfaces.**

I. Introduction

Wearable robots are an emerging technology in many fields such as rehabilitation, assistive devices, human augmentation, and haptics [1], [2], [3]. The physical human-robot interaction (pHRI) interface consists of the mechanical attachment between the user and the robot which is responsible for ensuring safe, comfortable, and effective force transfer [4]. Magnitude and distribution of pressures at the human-robot interface are critical factors in determining the comfort and safety of a wearable device [5]. Unsafe pressures can cause injury and degradation of tissue health, which is especially relevant in sensitive populations with a high rate of disuse of assistive devices [6]. Moreover, understanding and modeling the nature of interaction at the pHRI interface is critical for ensuring effective force transfer as intended by the device. This is relevant in all applications of wearable robots ranging from achieving intended task dynamics in haptics [7] to avoiding abnormal synergies in stroke patients undergoing rehabilitation [8].

The standard performance metric used to evaluate pHRI in the literature is single-point force/torque measurement at the human-robot interface, often obtained through a six-axis load cell located near the attachment [9], [10]. While such force/torque data provides valuable information about human-robot interaction at a macro level [10], [11], [12], it is insufficient for understanding the exact loads experienced by the human user distributed across the physical interface surface. Assuming six-axis force/torque measurements directly translate to loads sensed by the human incorrectly treats the pHRI attachment as a rigid connection, failing to consider compliance from human soft tissue and robot attachment materials. In reality, the stiffness of soft tissue at different locations on the human body plays an important role in determining behavior at human-robot interfaces [13], [14].

Recent developments in distributed sensing technologies [15], [16] present a promising solution for analyzing pHRI at the human-robot contact surface. However, such sensors can only provide information during or after the experiment and cannot always be integrated at human-robot interfaces. An analysis model can be used to determine distributed loads at the pHRI interface in advance based on expected interaction force/torque values. This can address the lack of distributed interface load sensing by providing researchers with better information in regards to forces transmitted to the human. Such an analysis framework can be used to predict distributed interface loads beforehand through simulation, enabling finer control of forces experienced by the human and allowing researchers to study which design factors optimize pHRI interfaces for comfortable and effective force transmission. While previous works have described trends in distributed measurements [15], [16], [17], no focused effort has been made to predict distributed interaction forces based on six-axis load cell measurements.

Building on Varghese et al. [14], our work analyzes the upper arm attachment interface (Fig. 1) with a pHRI model based on discretized elastic elements that account for human and robot compliance. The goal of the model is to predict

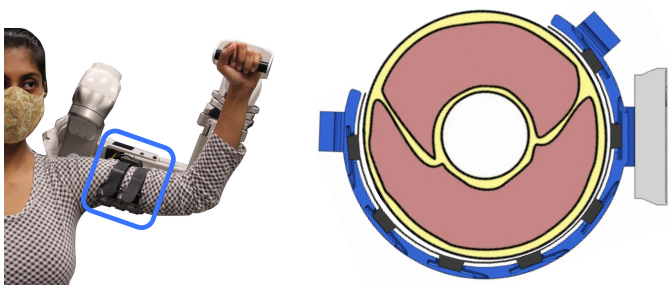

(a) Harmony exoskeleton (b) Upper arm cuff cross section

Fig. 1: The left arm of the Harmony upper limb exoskeleton. A cross section view of the highlighted upper arm pHRI interface is shown.

*A newer version of the indenter device used in this work is the subject of another AIM submission. That submission focuses on the design and control of the device and its broader applications.

This work was funded, in part, by the National Science Foundation (NSF) grant numbers 2019704 and 1941260, as well as the NSF Graduate Research Fellowship Program (GRFP) grant number DGE-1610403.

[1]S.N. Yousaf, P. Esmatloo, K. Ghonasgi, and A.D. Deshpande are with the Department of Mechanical Engineering, The University of Texas at Austin, TX 78712, USA. ashish@austin.utexas.edu

distributed loads at the human-robot interface based on general six-axis force/torque measurement at the attachment. The analysis presented in this paper shows that characterization of the surface compliance in the human limb leads to a more accurate pHRI interface model, resulting in improved prediction of distributed interface loads.

II. Methods

The analysis method discretizes the upper arm interface with either a rigid arm model or a compliant arm model (Fig. 2). A sensorized cuff measures the distributed loads transmitted across the discretized interface, and the level of compliance at each location in the model is based on stiffness measurements from an indenter device. The model is simulated given force/torque measurements from a load cell and calculates the distributed loading expected at the human-robot interface surface. Experiments conducted with the Harmony exoskeleton and a proxy upper arm made of polyethylene foam are used to validate the pHRI interface model's ability to predict distributed loads under two assumptions: a rigid upper arm and a compliant upper arm.

A. Sensorized Upper Arm Cuff for the Harmony Exoskeleton

Harmony is a powered bilateral exoskeleton designed for rehabilitation of shoulder and arm function [18] (Fig. 1a). It has been designed to apply controlled training protocols for rehabilitation such as repetition of passive movements with robot assistance [19]. In particular, this work focuses on the upper arm cuff attachment (Fig. 1b) which is one of Harmony's primary pHRI interfaces.

Most robots, including the Harmony exoskeleton, make use of single-point six-axis force/torque sensors to characterize interaction loads and are thus unable to capture the distribution of forces along the interface surface. Towards this detailed characterization of interaction at the human-robot interface, we have designed a sensorized upper arm cuff (Fig. 3) using force sensing resistors (FSRs) [20]. FSRs are able to measure surface forces and present a small footprint (diameter = 9.53mm), making them ideal for this application. Data collection from the FSRs was done through an NI-9205 module on an NI CompactRIO (National Instruments, Austin, TX) at a rate of

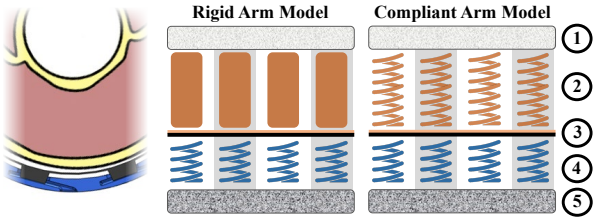

Fig. 2: The pHRI interface model of the upper arm attachment is used for analysis in simulation. The arm and cuff are modeled as discretized elastic elements in contact across the skin's interface surface. Elements of the schematic include: 1) rigid bone, 2) soft tissue stiffness, 3) skin surface, 4) cuff stiffness, and 5) rigid robot.

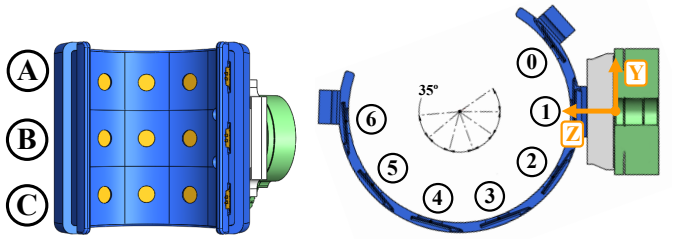

(a) Sensorized cuff top view (b) Sensorized cuff cross section

Fig. 3: The sensorized upper arm cuff (blue) is discretized into 21 sections. There are three rows labeled A, B, and C, with row A closest to the shoulder and row C closest to the elbow. There are seven angular locations spaced 35 degrees apart designated 0 through 6. The load cell (green) is mounted between the cuff and the robot as shown.

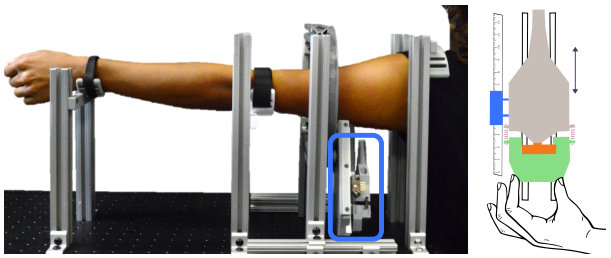

Fig. 4: Side view and functional schematic of the indenter device used to characterize stiffness of the upper arm. A linear encoder (blue) attached to the indenter head (brown) and a single-axis force sensor (orange) on a linear rail measure the force-displacement response.

100Hz. These sensors were calibrated prior to the experiment with an average load error of 0.35N $\pm$ 0.27N.

A total of 21 FSRs are installed in the sensorized upper arm cuff across three rows (Fig. 3a) and seven angular locations (Fig. 3b). The 21 FSR locations on the sensorized upper arm cuff define the discretization of the pHRI interface which is used during analysis. The cross section view (Fig. 3b) also highlights the placement of the six-axis load cell relative to the sensorized cuff which defines how force/torque measurements are transmitted to the pHRI interface in the model. This new design allows data collection from a number of points on the interface resulting in a complete picture of the load distribution across the cuff.

B. Indenter Device to Characterize Upper Arm Stiffness

To ensure comfortable and effective force transfer between the human and the robot, it is important to include viscoelastic properties of human soft tissue and the robot interface during analysis of force transmission. Indentation and tensile methods have been used to measure elastic properties of biological soft tissue [21] by relating tissue displacement to applied force. However, most in-vivo measurements have analyzed the elastic properties of the skin, focusing on micron-level displacements and small forces. In reality, forces transmitted between human users and wearable robotic devices can be much higher, and

there is a need to understand the properties of human tissue under higher ranges of force and displacement.

We have developed a custom device to measure stiffness from the force-displacement response of the human arm (Fig. 4). This device includes an indenter with customizable geometry that is mounted on a linear sliding rail. In this study, we use a cylindrical geometry (9mm diameter) and the stiffness value is converted into a distributed measurement across the contact surface area when used in the pHRI interface model. Linear displacement is measured using an EM1 optical encoder (US Digital, Vancouver, WA) with a resolution of 1/500 inch (0.025 mm), and applied force is measured using an FS20 single axis force sensor (TE Connectivity, Berwyn, PA). The location of indentation can be adjusted axially along the length of the arm or radially around the circumference of the arm. Data from the force sensor and the encoder are acquired using the NI-6356 module (National Instruments, Austin, TX). The displacement and force data are plotted using a MATLAB script in real-time during operation and saved for further analysis.

To measure surface stiffness of the arm, the subject is seated and the arm is secured inside the circular structure such that the humerus bone is approximately centered. In the case of a proxy upper arm, both ends of the rigid bone structure are mounted and measurements are made on the soft foam surface. An operator moves the indenter to the appropriate position around the arm where the stiffness value is of interest. These locations correspond to the 21 discretized segments from the upper arm cuff (Fig. 3b) with measurements at seven angles across three rows. The operator manually indents the arm while monitoring the applied force in real time and repeats the process twice at each discretized location. The force is zeroed during the first three seconds of the trial, and the indentation onset is determined using a difference threshold for the force value.

C. Simulation Based on Human-Robot Interface Model

The pHRI interface is modeled as a physical system with compliant elements (Fig. 2). The rigid bones of the human skeleton and the rigid links of the robot act as ground reference structures. The stiffness of the soft tissue in the upper arm and the stiffness of the robot's cuff are both assumed to behave as a set of elastic springs in series. The strap pretension is taken into account by applying a fixed force at the strap handles on the upper arm cuff. The current pHRI model does not include soft tissue damping properties. While they will be included in future dynamic simulation models, viscoelastic relaxation through indentation has shown that elastic properties capture the majority of soft tissue behavior [21]. However, muscle contraction plays a bigger role in interaction behavior and is a limitation of this model. Future efforts will incorporate muscle activation and its effect on viscoelastic properties at the interface.

This model is simulated in SolidWorks 2020 (Dassault Systèmes SolidWorks Corporation, Waltham, MA) as a finite element analysis (FEA) based on a linear static study [22] developed with the CAD of the upper arm cuff and its interfacing components. The soft tissue stiffness is defined uniquely for each location throughout the discretized interface surface as individual elastic supports based on measurements from the indenter device. The cuff stiffness is captured in the CAD model and determined by material properties. The inputs for the simulation are the six-axis interaction forces/torques as well as the strap pretension. The outputs from the simulation are the distributed loads measured at each location on the discretized interface surface. While this study considers 21 locations on the upper arm pHRI interface, the level of discretization can be adjusted in the simulation depending on the desired analysis.

III. Experiment Design

Experiments were performed with the Harmony exoskeleton and a proxy upper arm (Fig. 5). The proxy arm is built with polyethylene foam which possesses compliant properties that are comparable to those of soft tissues on a human arm. The polyethylene foam is mounted on a rigid cylindrical core that replicates the grounding location of a rigid human bone. The use of a proxy upper arm ensures stiffness doesn't change over time and serves as the first step in validation of our pHRI interface model. This approach is inspired by similar methods used in previous pHRI research [23], [24]. Future human subject testing will account for changing stiffness of the upper arm due to muscle contraction, viscous properties of soft tissue, and other biomechanical effects.

Two experimental protocols were used to explore pHRI at the upper arm interface. In each protocol, the Harmony exoskeleton starts at the same home position, and the strap pretension at the upper arm cuff is measured to be $15N \pm 0.1N$. The human-robot attachment interface is loaded in two different directions within each experimental protocol. In reference to Fig. 3b, vertical loading corresponds to the y-axis of the load cell, and horizontal loading corresponds to the z-axis. Time series data recorded for experiments include single-point six-axis load cell measurements and distributed interaction forces from the 21 FSRs on the sensorized cuff.

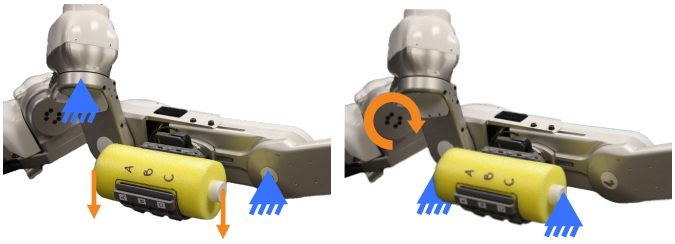

(a) I-Act (b) II-Pass

Fig. 5: Experiment setup with the proxy upper arm and the Harmony exoskeleton (cuff straps not shown). In the active experiment (I-Act), the proxy upper arm is loaded while the robot is grounded. In the passive experiment (II-Pass), the proxy upper arm is grounded while the robot is actuated.

A. Experiment I-Act: Active Subject with Proxy Arm Loading

In the first experiment, the Harmony exoskeleton is fixed at its home position, and the proxy upper arm is loaded either horizontally or vertically (Fig. 5a). Three different loads (11.1N, 33.4N, and 55.6N) are applied by hanging weights, and a pulley system is used for horizontal loading. This experiment imitates active movement of a human subject against a robot and is labeled I-Act.

B. Experiment II-Pass: Passive Subject with Robot Actuation

In the second experiment, the proxy upper arm is grounded, and the Harmony exoskeleton is actuated at the shoulder joint (Fig. 5b). Two types of shoulder actuation are performed: horizontal abduction-adduction or vertical flexion-extension. Each actuator rotates through 10 degrees and imparts a corresponding horizontal or vertical load at the pHRI interface. This experiment corresponds to a passive human user whose movement is driven by a robot providing assistance and is labeled II-Pass.

C. Experiment Setup in Simulation

Both the active (I-Act) and passive (II-Pass) experiments are analyzed via simulation as described in section II-C. First, the simulation is processed assuming a rigid upper arm such that the soft tissue elastic elements (Fig. 2) are fixed. Next, the proxy upper arm stiffness values measured by the indenter device introduced in section II-B are included in the model, and a second set of simulations is performed assuming a compliant upper arm.

For the active experiment (I-Act), each type of simulation is performed four times in total: once during the no load condition and once during each of the three loading conditions. For the passive experiment (II-Pass), each simulation is performed once before the robot is actuated and once at each of three points in the robot's actuation when the sinusoidal joint trajectory is at the minimum, midpoint, and maximum. The experimentally measured distributed loads are calibrated to zero based on the initial offset measured during the no loading period. Similarly, the distributed loads from the simulation output are calibrated to zero based on the simulation results for the no load condition. For both experiments, three trials are considered for each loading or actuation condition.

IV. Results

A. Upper Arm Surface Stiffness

The force-displacement response of the proxy upper arm is relatively linear with a mild hysteresis effect (Fig. 6a). Stiffness was calculated as the average of the slopes from lines fitted to the unloading plots. While the loading and unloading curves have similar slopes, the unloading data are preferred in literature [14] and represent a closer approximation of the proxy arm when it is preloaded by the cuff during experiments. The calculated stiffness values at the 21 points around the proxy arm surface are shown in Fig. 6b. As expected, the stiffness values are similar across the proxy arm and average to 4242N/m±251.5N/m.

B. Simulation Performance: Rigid Arm and Compliant Arm

The goal of the pHRI model in simulation is to predict distributed interface loads measured by the sensorized upper arm cuff during experimentation. Thus, the root mean square error (RMSE) is computed by comparing experimental FSR data with simulation output based on Eq. 1 where the discretized location is represented by $i = A,B,C$ corresponding to the row and $j = 0,1,2,...,6$ corresponding to the angular position on the cuff (Fig. 3). In this case, $N = 21$ given the 21 discretized locations on the upper arm interface. For each loading condition within each experiment, two RMSE values are computed for each trial. The first compares the simulation with a rigid arm to experimental data while the second compares the simulation with a compliant arm to the same experimental data. The RMSE values are shown in Fig. 7a (I-Act) and Fig. 7b (II-Pass).

$$RMSE = \sqrt{\frac{\sum_{i,j}\left(F_{i,j}^{expt} - F_{i,j}^{sim}\right)^2}{N}} \tag{1}$$

The distributed interface loads are visualized as heat maps of forces across the 21 discretized locations to observe trends within data. Fig. 8a shows the six-axis force/torque measurements during the active experiment (I-Act) for horizontal loading at the second load, 33.4N, during the first trial. Fig. 8b shows heat maps that represent the corresponding distributed loads from experimental and simulation data. The first heat map shows experimental data collected by the sensorized upper arm cuff. The second heat map shows simulation data with a rigid upper arm, whereas the third heat map shows simulation data with a compliant upper arm.

V. Discussion

Since pHRI interfaces are critical points of interaction between the human and the robot, it is imperative to accurately monitor and control the behavior they impose to ensure comfort and safety of the human user. We introduce an interface model in simulation that uses six-axis load cell

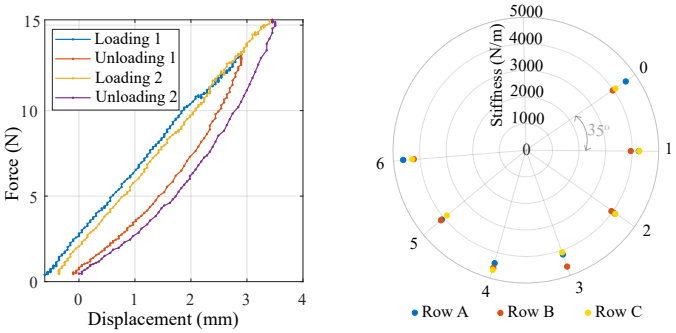

(a) Proxy arm indentation (b) Proxy arm stiffness profile

Fig. 6: A sample indentation response for the proxy arm and the measured stiffness values around the proxy arm surface for three rows (A,B,C) and 7 angular locations (0,1,...,6).

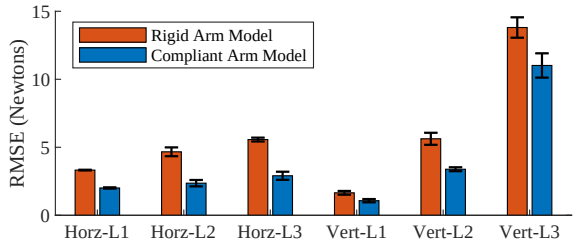

(a) I-Act Experiment

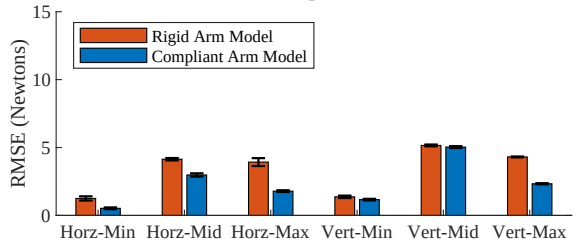

(b) II-Pass Experiment

Fig. 7: Bar plots of the RMSE comparing predicted distributed loads from simulation to measured distributed loads from the sensorized cuff. Each bar represents the average RMSE of three trials at that loading condition, and the error bars show the standard error for RMSE across three trials. L1, L2, and L3 correspond to the three load levels (11.1N, 33.4N, and 55.6N).

measurements from the Harmony exoskeleton and stiffness values for the proxy upper arm to predict distributed loads across the upper arm cuff interface. Two simulation versions are used to explore the rigid arm assumption and the compliant arm assumption. We compare the performance of each version of the simulation to experimentally collected load distributions from the sensorized upper arm cuff.

The results from the simulation with a rigid upper arm assumption can be observed from the respective RMSE values (Fig. 7a and Fig. 7b). While this simulation predicts the general trends observed in experimental data, the RMSE values approach 5N in many loading cases and even reach up to 13N. High RMSE values indicate inaccurate prediction of pHRI interface forces which can lead to dangerous loads at the human surface. For context, pain pressure threshold (PPT) is a clinical metric used to define the minimum force which induces pain. While PPT measures vary, the lowest upper arm PPT based on [25] is 120kPa, corresponding to a maximum force of 84N at a discretized location. Thus, the high RMSE values observed in the rigid arm simulation approach 15% of the maximum accepted load, making it increasingly unreliable to maintain user safety while optimizing device performance.

In Fig. 8b, the horizontal loading case with forces applied in the z-axis of the load cell (see Fig. 3b) is shown, where most of the distributed interface loads are expected to be at angular locations 5 and 6 with unloading expected at locations 0 and 1. This is evident on the first heat map representing experimental data from the sensorized cuff. As evident by the second heat map (Fig. 8b), the simulation with a rigid arm not only predicts high loads but incorrectly concentrates all of

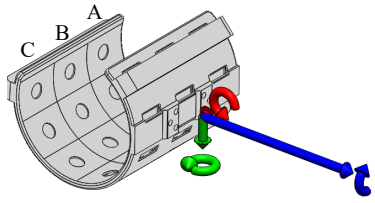

(a) Six-axis load cell measurement

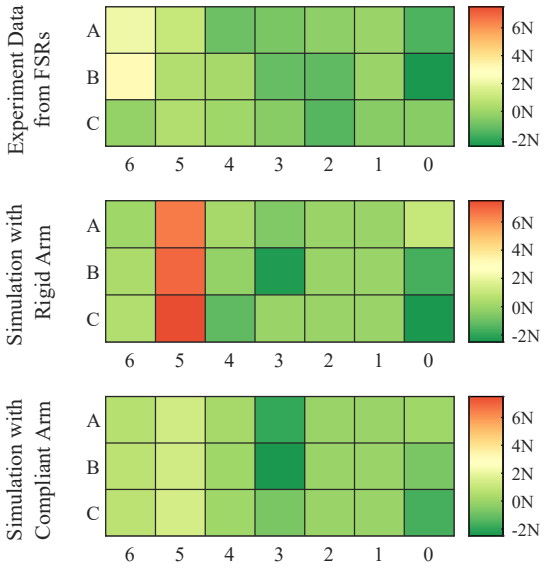

(b) Distributed loads at 21 discretized locations

Fig. 8: The active experiment (I-Act) with the horizontal loading of the proxy arm at the second load (33.4N) is shown. Six-axis load cell measurements are illustrated in the x (red), y (green), and z (blue) axes. Heat maps show corresponding experiment and simulation results. The first heat map illustrates experimental data measured from the sensorized upper arm cuff. The second and third heat maps show simulation data for the rigid arm and compliant arm cases, respectively. The vertical axes correspond to rows of the pHRI interface (Fig. 3a), and the columns correspond to angular locations at the pHRI interface (Fig. 3b).

them at angular location 5. Similar errors are observed across loading cases. Given the mediocre performance of the rigid arm simulation, it becomes apparent that elastic properties of the proxy upper arm must be characterized to build a better pHRI interface model.

The second analysis conducted with the compliant arm simulation includes measured discretized stiffness values of the proxy upper arm (Fig. 6b). The RMSE values (Fig. 7) indicate that our proposed compliant arm simulation performs better at predicting distributed loads at the pHRI interface compared to the simpler rigid arm simulation. Further inspection of the third heat map (Fig. 8b) shows that compliant modeling of the upper arm helps the simulation predict accurate loading at angular location 5. Similar trends for the compliant arm simulation are observed at other load conditions.

In both experiments (I-Act and II-Pass), the RMSE values

show a positive correlation with increasing load or level of actuation. This might be explained by losses during force transmission at the pHRI interface which are not captured by the model during simulation. Another possible source of discrepancy is the sensorized upper arm cuff and how it is modeled. While the simulation assumes all loads are transmitted through the FSRs, as was the intention with the sensorized cuff design, it is likely that at least some loads are transmitted onto other surfaces. Future work will aim to address this shortcoming with better design and modeling.

Lastly, the vertical loading condition during the active experiment (I-Act) stands out because of the high RMSE values at high loads. Even analysis with a compliant upper arm fails to accurately predict distributed interface loading in this scenario. A likely explanation for this error comes from the impedance control of the robot resulting in unintended movement of robot joints leading to unexpected movement in the arm in response to large loads. Inconsistency from the velcro strap is another potential source of error. While loading in the horizontal direction mainly manifests on the sides of the cuff itself, loading in the vertical direction has more influence from strap forces. Thus, strap material properties and initial pretension become more relevant in this loading condition.

VI. Conclusion

In this paper, we show that a pHRI model allows us to understand how forces and torques are transmitted across the human-robot interface surface as distributed loads. We also demonstrated that our proposed approach for modeling the pHRI interface with compliant properties of the limb leads to a better estimation of distributed loads at the attachment as compared to the rigid connection assumption. This study underscores the need for distributed measurement to understand the fine nature of forces directly at the location of interaction. Future work will extend this pHRI analysis to include human subject testing and dynamic loading conditions. This approach lays the groundwork for modeling physical human-robot interaction which is critical for the next generation of wearable devices designed to integrate with human users.

References

[1] S. Viteckova, P. Kutilek, and M. Jirina, "Wearable lower limb robotics: A review," *Biocybernetics and Biomedical Engineering*, vol. 33, no. 2, pp. 96–105, 2013.

[2] P. Maciejasz, J. Eschweiler, K. Gerlach-Hahn, A. Jansen-Troy, and S. Leonhardt, "A survey on robotic devices for upper limb rehabilitation," *Journal of neuroengineering and rehabilitation*, vol. 11, no. 1, p. 3, 2014.

[3] A. M. Dollar and H. Herr, "Lower extremity exoskeletons and active orthoses: Challenges and state-of-the-art," *IEEE Transactions on robotics*, vol. 24, no. 1, pp. 144–158, 2008.

[4] A. De Santis, B. Siciliano, A. De Luca, and A. Bicchi, "An atlas of physical human–robot interaction," *Mechanism and Machine Theory*, vol. 43, no. 3, pp. 253–270, 2008.

[5] E. Rocon, A. Ruiz, R. Raya, A. Schiele, J. L. Pons, J. Belda-Lois, R. Poveda, M. Vivas, and J. Moreno, "Human-robot physical interaction," *Wearable robots: Biomechatronic exoskeletons*, pp. 127–163, 2008.

[6] E. Biddiss and T. Chau, "Upper-limb prosthetics: critical factors in device abandonment," *American journal of physical medicine & rehabilitation*, vol. 86, no. 12, pp. 977–987, 2007.

[7] E. Pezent, S. Fani, J. Clark, M. Bianchi, and M. K. O'Malley, "Spatially separating haptic guidance from task dynamics through wearable devices," *IEEE transactions on haptics*, vol. 12, no. 4, pp. 581–593, 2019.

[8] P.-C. Kung, C.-C. K. Lin, and M.-S. Ju, "Neuro-rehabilitation robot-assisted assessments of synergy patterns of forearm, elbow and shoulder joints in chronic stroke patients," *Clinical Biomechanics*, vol. 25, no. 7, pp. 647–654, 2010.

[9] A. Schiele, "Ergonomics of exoskeletons: Objective performance metrics," in *World Haptics 2009-Third Joint EuroHaptics conference and Symposium on Haptic Interfaces for Virtual Environment and Teleoperator Systems*. IEEE, 2009, pp. 103–108.

[10] N. Jarrassé and G. Morel, "Connecting a human limb to an exoskeleton," *IEEE Transactions on Robotics*, vol. 28, no. 3, pp. 697–709, 2011.

[11] A. Schiele and F. C. Van Der Helm, "Kinematic design to improve ergonomics in human machine interaction," *IEEE Transactions on neural systems and rehabilitation engineering*, vol. 14, no. 4, pp. 456–469, 2006.

[12] D. Accoto, F. Sergi, N. L. Tagliamonte, G. Carpino, A. Sudano, and E. Guglielmelli, "Robomorphism: a nonanthropomorphic wearable robot," *IEEE Robotics & Automation Magazine*, vol. 21, no. 4, pp. 45–55, 2014.

[13] D. M. Sengeh and H. Herr, "A variable-impedance prosthetic socket for a transtibial amputee designed from magnetic resonance imaging data," *JPO: Journal of Prosthetics and Orthotics*, vol. 25, no. 3, pp. 129–137, 2013.

[14] R. J. Varghese, G. Mukherjee, R. King, S. Keller, and A. D. Deshpande, "Designing variable stiffness profiles to optimize the physical human robot interface of hand exoskeletons," in *2018 7th IEEE International Conference on Biomedical Robotics and Biomechatronics (Biorob)*. IEEE, 2018, pp. 1101–1108.

[15] M. Donati, N. Vitiello, S. M. M. De Rossi, T. Lenzi, S. Crea, A. Persichetti, F. Giovacchini, B. Koopman, J. Podobnik, M. Munih *et al.*, "A flexible sensor technology for the distributed measurement of interaction pressure," *Sensors*, vol. 13, no. 1, pp. 1021–1045, 2013.

[16] J. Tamez-Duque, R. Cobian-Ugalde, A. Kilicarslan, A. Venkatakrishnan, R. Soto, and J. L. Contreras-Vidal, "Real-time strap pressure sensor system for powered exoskeletons," *Sensors*, vol. 15, no. 2, pp. 4550–4563, 2015.

[17] A. Rathore, M. Wilcox, D. Z. M. Ramirez, R. Loureiro, and T. Carlson, "Quantifying the human-robot interaction forces between a lower limb exoskeleton and healthy users," in *2016 38th Annual International Conference of the IEEE Engineering in Medicine and Biology Society (EMBC)*. IEEE, 2016, pp. 586–589.

[18] B. Kim and A. D. Deshpande, "An upper-body rehabilitation exoskeleton harmony with an anatomical shoulder mechanism: Design, modeling, control, and performance evaluation," *The International Journal of Robotics Research*, vol. 36, no. 4, pp. 414–435, 2017.

[19] A. C. de Oliveira, C. G. Rose, K. Warburton, E. M. Ogden, B. Whitford, R. K. Lee, and A. D. Deshpande, "Exploring the capabilities of harmony for upper-limb stroke therapy," in *2019 IEEE 16th International Conference on Rehabilitation Robotics (ICORR)*. IEEE, 2019, pp. 637–643.

[20] K. Ghonasgi, S. N. Yousaf, P. Esmatloo, and A. D. Deshpande, "A modular design for distributed measurement of human–robot interaction forces in wearable devices," *Sensors*, vol. 21, no. 4, p. 1445, 2021.

[21] A. Petron, J.-F. Duval, and H. Herr, "Multi-indenter device forin vivobiomechanical tissue measurement," *IEEE Transactions on Neural Systems and Rehabilitation Engineering*, vol. 25, no. 5, pp. 426–435, 2016.

[22] R. Shih, *Introduction to finite element analysis using solidworks simulation 2014*. SDC publications, 2014.

[23] A. B. Ambrose and F. L. Hammond, "Soft pneumatic system for interface pressure regulation and automated hands-free donning in robotic prostheses," in *2020 IEEE International Conference on Robotics and Automation (ICRA)*. IEEE, 2020, pp. 4848–4854.

[24] S. N. Yousaf, V. S. Joshi, J. E. Britt, C. G. Rose, and M. K. O'Malley, "Design and characterization of a passive instrumented hand," *ASME Letters in Dynamic Systems and Control*, vol. 1, no. 1.

[25] D. H. Jones, R. D. Kilgour, and A. S. Comtois, "Test-retest reliability of pressure pain threshold measurements of the upper limb and torso in young healthy women," *The Journal of Pain*, vol. 8, no. 8, pp. 650–656, 2007.